



Understanding the black hole–galaxy connection: a multi-X-ray observatory approach

S. Marchesi^{1,2}

¹ INAF - Osservatorio di Astrofisica e Scienza dello Spazio di Bologna, Via Piero Gobetti, 93/3, 40129, Bologna, Italy

² Department of Physics and Astronomy, Clemson University, Kinard Lab of Physics, Clemson, SC 29634, USA

Abstract. An accurate census and characterization of accreting supermassive black holes (SMBHs) over cosmic time, both in the local Universe and at very high redshift, can be efficiently achieved through a synergy between the different X-ray facilities currently available. For example, deep surveys with *Chandra* in the 0.5–7 keV band, such as the one performed over the 2.2 deg² COSMOS field, allow one to detect thousands of active galactic nuclei (AGN) at luminosities that are almost completely below the knee of the luminosity function. Consequently, such X-ray surveys can sample the typical AGN population up to $z \sim 6$, detecting a large number of obscured AGN that would otherwise be missed by optical surveys.

Thanks to X-ray surveys, it is well known that the vast majority of SMBHs in the center of galaxies accrete material in an obscured phase, where the obscuration is caused by a nuclear-scale distribution of matter with column density $N_{\text{H},z} > 10^{22} \text{ cm}^{-2}$ which is possibly a reservoir of gas for the SMBH accretion. For this reason, a full understanding of SMBH accretion and of his effects on the host galaxy requires *i*) a detailed study of the obscuring material, i.e., a complete characterization of its geometrical, chemical and kinematical properties, and *ii*) a systematic comparison between observations and hydrodynamical simulations of active galactic nuclei (AGN) feeding and feedback. These goals can be best addressed studying a large sample of nearby, heavily obscured AGN with high-quality *NuSTAR* data in the 3–70 keV band, ideally combined with infrared/mm observations to complement the X-ray data.

Next generation X-ray facilities, such as *Athena* and the proposed *Lynx* and *AXIS* missions, will build on the results obtained by current X-ray facilities. In particular, these new observatories will discover a new population of $z > 6$ sources, thus providing key constraints to theoretical models of black hole seeds and early SMBH growth.

Key words. X-rays: galaxies – Surveys – Galaxies: active – Galaxies: Seyfert

1. Introduction

One of the most active but least known epochs in astrophysics is the period between re-ionization ($z \geq 8$), where the growth of struc-

tures becomes highly non-linear and the first stars form, and $z \sim 2$, where major virialization occurs and star formation (SF) and supermassive black hole (SMBH) accretion peak. Most SMBHs - and definitely the most massive ones

- had to grow during an active accretion phase, when they would be visible as an active galactic nucleus (AGN), implying that most galaxies had an AGN phase in their past.

While we have a clear view on the tight relation between SMBH and host properties, several questions are still open on the way SMBHs and galaxy evolved from the early universe. For example, which is the black hole (BH) main accretion scenario? Did the BH grow first, at accretion rates close to the maximum allowed, possibly driven by major mergers? Or did the growth of the BH followed the one of the galaxy, through secular accretion? Or did galaxy and BH grow in symbiosis? How significantly do AGN contribute to the Hydrogen (HI) reionization when the Universe was less than 1 Byr old, at $z \sim 6$? Which is the role played by obscured and Compton thick AGN? Does their contribution significantly change in different epochs? What does the characterization of heavily obscured AGN in the local Universe tell us on the final phases of SMBH growth, and how is this information tied to the higher redshift one?

All these questions can be addressed by a multi-X-ray observatory approach, aimed at combining in an efficient synergy the different observatories which are looking at the sky in the 0.3–150 keV energy range.

1.1. The key role of X-ray surveys in characterizing the SMBH-galaxy co-evolution

The co-evolution of SMBH and galaxies can be studied using sizable samples of AGN, both obscured and unobscured, with multi-wavelength data to observe both SMBH and galaxy emission. To access the moderate luminosity AGN that dominate the X-ray background (CXB) requires a deep moderate-area survey ($\geq 1 \text{ deg}^2$ in area, at sufficient depth to detect AGN at $z \leq 6$), while large area surveys in the hard X-rays ($E > 10 \text{ keV}$) are strategic to study and put better constraints on the most heavily obscured AGN, the Compton thick ones (CT; i.e., sources with column density $N_H > 10^{24} \text{ cm}^{-2}$). X-ray data play an important

role in the selection of AGN, for two main reasons:

1. At X-ray energies the contamination from non-active galaxies, many of which are star-forming, is far less significant than in optical and infrared surveys (Donley et al. 2008, 2012; Stern et al. 2012; Lehmer et al. 2012).
2. X-ray surveys with *Chandra* and XMM-Newton are very effective in selecting both unobscured and obscured AGN, including also Compton thick sources (i.e., with hydrogen column densities, N_H , up to 10^{24} cm^{-2}), at $z \approx 1\text{--}2$ (Comastri et al. 2011; Georgantopoulos et al. 2013; Lanzuisi et al. 2015). Complementary results have been obtained by works with the hard X-ray telescope Nuclear Spectroscopic Telescope Array (*NuSTAR*, Harrison et al. 2013), which covers the 3–78 keV energy range and has been proved extremely effective in detecting candidate sources (undetected by *Chandra* and XMM-Newton) above the 10^{24} cm^{-2} threshold at redshift $z < 1$ (Del Moro et al. 2014; Lansbury et al. 2014; Civano et al. 2015) and in characterizing already known candidate CT-AGNs in the nearby Universe ($z < 0.1$; see, e.g., Puccetti et al. 2014; Brightman et al. 2015; Masini et al. 2016; Marchesi et al. 2018, 2019a; Zhao et al. 2019b,a).

In the next sections, I will present the main recent results on the study of AGNs growth and evolution from an X-ray perspective, with a particular focus on the projects in which I have been directly involved.

2. Mapping obscured accreting supermassive black holes with large X-ray surveys

The *Chandra COSMOS-Legacy* survey (Civano et al. 2016; Marchesi et al. 2016a) is a 4.6 Ms *Chandra* survey in the 0.5–7 keV band. It covers a 2.2 deg^2 area, reaching a flux limit in the 0.5–2 keV band $f_{0.5-2} = 2 \times 10^{-16} \text{ erg s}^{-1} \text{ cm}^{-2}$. *COSMOS-Legacy* explores a new region of the area-flux parameter space for X-ray surveys, being an additional factor 2–3 deeper than other surveys at the same covered area: this result is obtained

using a total exposure time which is unusually large for that given area flux combination, thus opening the path for surveys with future facilities.

The *Chandra COSMOS-Legacy* catalog contains over 4000 point-like X-ray sources, 20–35 % more than other contiguous surveys with similar area (e.g. 3362 sources in Stripe 82; 2976 in X-DEEP2). The plethora of multiwavelength data available in the COSMOS field allows us to compute a photometric redshift for 97% of the *Chandra COSMOS-Legacy* sources, all optically/infrared (IR) identified (Marchesi et al. 2016a). At the *Chandra COSMOS-Legacy* fluxes, 70% of the sources are optically obscured, setting the stage for studying host galaxy properties with no contamination from the active BH, which can instead be fully characterized with the X-ray data. Moreover, as shown in Figure 1, left panel, more than 90% of the *Chandra COSMOS-Legacy* sources are below the knee of the luminosity function at any redshift, thus probing the faint end of the AGN population which is missed by both optical and shallower X-ray surveys.

The *Chandra COSMOS-Legacy* sample also contains ~2000 objects that are bright enough (i.e., have ≥ 30 net counts in the 0.5–7 keV band) to perform a X-ray spectral analysis: the results of this analysis are reported in Marchesi et al. (2016c). One of the main topics of interest was to determine if optically classified Type 1 and Type2 AGN have different X-ray spectral properties, taking full advantage of both the X-ray and optical/IR photometric and spectroscopic coverage of the COSMOS field.

We find that, as expected, optically classified Type 2 AGN are on average three times more obscured than Type 1 AGN: however, ~15% of Type 1 AGN are obscured (i.e., have line-of-sight column density $N_{\text{H},z} > 10^{22} \text{ cm}^{-2}$), while ~20% of Type 2 AGN are unobscured. The first result suggest that the X-ray and optical obscuration can be at least partially caused by different phenomena, potentially happening at different spatial scales; since most of the unobscured Type 2 AGN also have low luminosities, the second result can instead be explained with a fraction of Type 2 AGN be-

ing low-accretion, unobscured AGNs lacking broad emission lines.

Finally, the existence or lack of a relation between $N_{\text{H},z}$ and the host-galaxy mass (M_*), star formation rate (SFR) and specific star formation rate (sSFR) has been largely discussed in the past ~10 years. Several works find no evidence of correlation between $N_{\text{H},z}$ and these host-related quantities (e.g., Shao et al. 2010; Rovilos et al. 2012; Rosario et al. 2012), while several others find a positive correlation with M_* (e.g., Rodighiero et al. 2015; Lanzuisi et al. 2017), in some cases directly linking the measured $N_{\text{H},z}$ with the amount of gas in the host (e.g., Circosta et al. 2019). In *Chandra COSMOS-Legacy* we find tentative evidence of a direct, proportional trend between $N_{\text{H},z}$ and the host-galaxy mass and star formation rate (see Figure 1, right panel). This result is partially driven by a redshift selection effect, but it still supports a scenario where more obscured AGN are located in more massive and (particularly) more star-forming galaxies. This suggests that part of the obscuration could be off-nuclear and caused by the gas-rich material responsible for the star formation.

2.1. Testing the BH formation scenario and the role of AGN in HI reionization with *Chandra COSMOS-Legacy*

The largest sample of X-ray selected high-redshift AGN on a contiguous field is contained in *Chandra COSMOS-Legacy*, with 174 sources at $z \geq 3$. As a comparison, the Vito et al. (2014) sample, obtained combining different surveys, contained 141 sources. The study of the *Chandra COSMOS-Legacy* $z > 3$ sample is presented in Marchesi et al. (2016b); I summarize here the main results of this paper.

The rest frame 2-10 keV comoving space density at $z \geq 3$ can be used to put constraints on the BH formation scenario. In fact, the shape of the space density is linked to the time-scale of accretion of SMBHs and it is therefore a tool to investigate the SMBH formation and growth scenario, eventually distinguishing between major-merger driven accretion and sec-

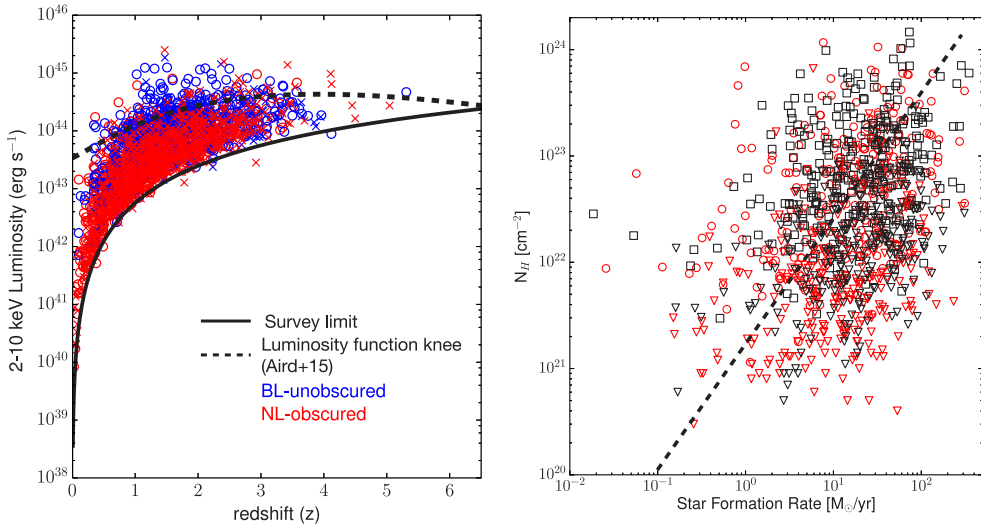


Fig. 1. *Left:* 2–10 keV rest-frame luminosity versus redshift for the AGN in the *Chandra COSMOS-Legacy* survey. Blue sources are either broad-line or unobscured AGN, red sources are narrow-line or obscured AGN; the information is derived from optical spectroscopy and from spectral energy distribution fitting, respectively. The survey flux limit (black solid line) and the L^* curve as function of redshift from Aird et al. (2015, black dashed line) are also shown. *Right:* Intrinsic absorption $N_{\mathrm{H},z}$ as a function of the star formation rate for the optically classified Type 2 AGN with more than 30 net counts in *Chandra COSMOS-Legacy*. Sources spectroscopically classified are plotted as red circles, while sources with only SED template best-fitting information are plotted as black squares. Upper limits on $N_{\mathrm{H},z}$ are plotted as triangles. The linear best-fit correlation is shown as a dashed black line. More obscured AGN are, on average, located in gas-rich, more star-forming galaxies.

ular accretion. In the survey high luminosity range ($L_X \geq L^*$), our data show a clear decline, consistent with the one observed in optical surveys at higher luminosities (e.g. Masters et al. 2012; McGreer et al. 2013) and predicted by different CXB synthesis models (e.g., Gilli et al. 2007; Ueda et al. 2014; Aird et al. 2015). Interestingly, a potential flattening in the decline at $z > 4$ is also measured. Dividing our sample in unobscured and obscured AGN (ss shown in Figure 2, left panel) we find that the flattening is almost entirely due to obscured sources, the unobscured sources instead having a slope in agreement with the one of the models. The ratio between obscured and unobscured sources is ≈ 1 in the redshift range $z=[3-4]$, while it grows to ≈ 2 at $z=5$. The evidence of an increasing fraction of obscured sources

at high redshifts was shown in other works (e.g., La Franca et al. 2005; Ballantyne et al. 2006; Hasinger 2008; Lanzuisi et al. 2018). Obscuration could in fact be linked to a major-merger AGN evolutionary scenario (Alexander & Hickox 2012); however, in our sample only a small fraction of sources (<20%) show clear evidence of merging.

To further explore the role of galaxy merging in triggering AGN activity, we also compared our data with the models of BH activation through major merger of (Shen 2009). These models have been calibrated on optical AGN surveys (Ross et al. 2013), at luminosities a factor of 10 higher than those of *Chandra COSMOS-Legacy* ($L_{\mathrm{bol}} > 10^{46} \text{ erg s}^{-1}$). As shown in Figure 2, right panel, this model strongly overpredicts our newest num-

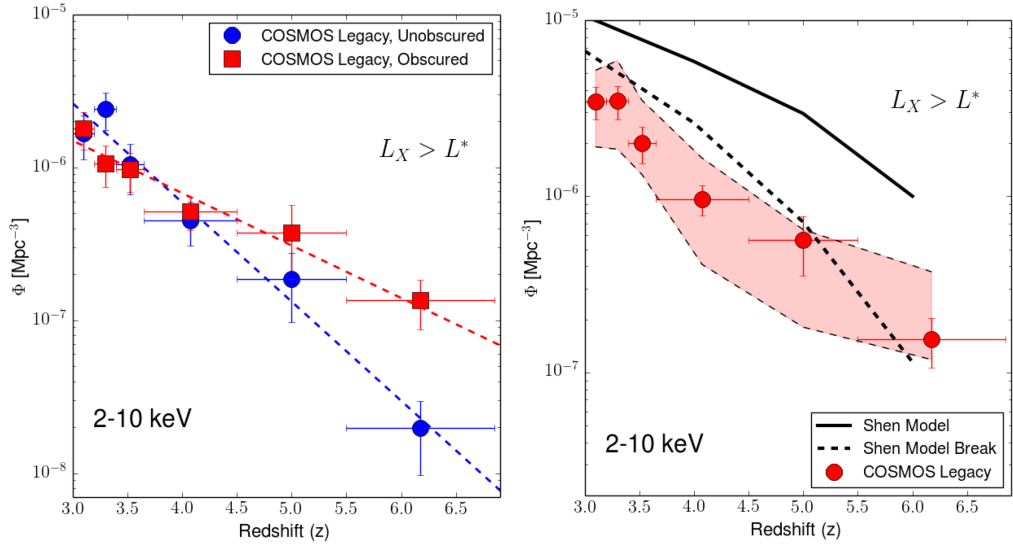


Fig. 2. *Left:* Space density of *Chandra COSMOS-Legacy* photometrically/spectroscopically classified unobscured (blue dots) and obscured (red squares) sources. Moving towards higher redshifts, the fraction of obscured AGN seem to increase. *Right:* Space density compared with the basic BH activation through major merger model from Shen (2009, black solid line) and with a modified version of the same model (black dashed line). The pale red area delimits the upper and lower limits of the *Chandra COSMOS-Legacy* space density. The plot clearly shows how X-ray selected, less luminous AGN tend to favor a secular accretion scenario over a major merger one.

ber counts at faint luminosities by a factor of 3-10. Such a result is mainly due to the model being calibrated at high luminosities, and then extrapolated to the luminosity range we analyzed. At high luminosities, major-merger activated AGN are expected to be dominant; in our sample, only a minority of sources show merging evidence. This simple exercise on the AGN space density lead us to the strong evidence that in our luminosity range the secular accretion scenario is preferred. This result is in agreement with those obtained by more sophisticated works, like those of Allevato et al. (2014, 2016, 2019), based on the AGN clustering, or the one of Cisternas et al. (2013), based on galaxy morphology.

Finally, in Ricci et al. (2017) we used the *Chandra COSMOS-Legacy* X-ray luminosity function (XLF) at $z>3$ to put stronger constraints on the ultraviolet (UV)/optical AGN LF, since the X-ray selection is less biased and allows one to reach fainter luminosities

than the UV one. We then used our results to derive the comoving QSO emissivity up to $z\sim 5$, extending at ~ 5 lower magnitudes than the limits probed by current UV/optical LFs, and to measure the contribution of AGN to HI ionization at $z\sim 6$. We found that at $z\sim 6$ AGN only marginally contribute to the ionization ($\sim 1-7\%$), thus reliably ruling out an AGN-dominated reionization scenario. Such a result is in disagreement with recent works which predicted a significant role of AGN in the ionizing process (e.g., Giallongo et al. 2015; Madau & Haardt 2015).

3. A multi-X-ray observatory approach to characterize heavily obscured AGN in the nearby Universe

Based on AGN population synthesis models (see, e.g., Gilli et al. 2007; Ueda et al. 2014; Buchner et al. 2015; Ananna et al. 2019),

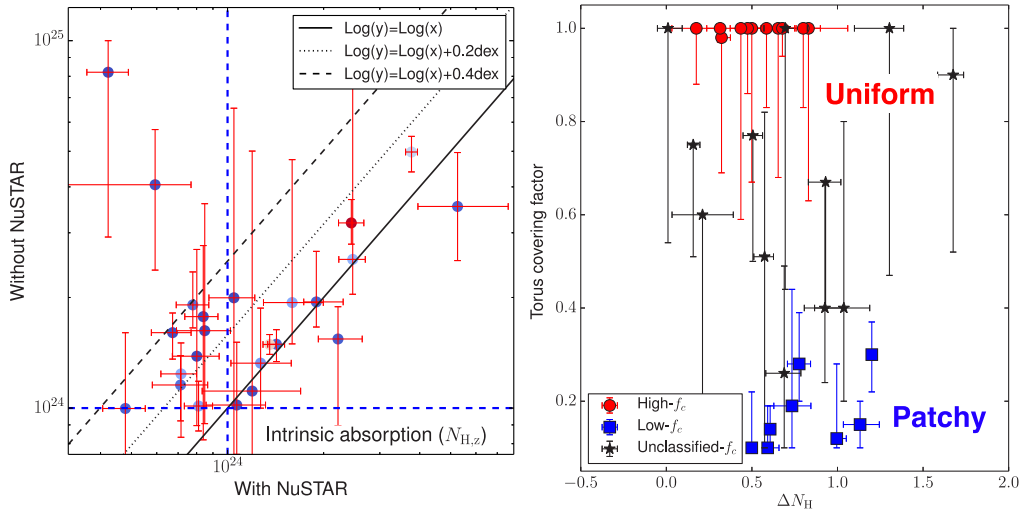


Fig. 3. *Left:* Distribution of the l.o.s. column density measured without the *NuSTAR* contribution as a function of the same parameter measured including the *NuSTAR* data to the fit for 28 candidate CT-AGN in the 100-month BAT catalog (Marchesi et al. 2018). The $\text{Log}(y)=\text{Log}(x)$, $\text{Log}(y)=\text{Log}(x)+0.2 \text{ dex}$ and $\text{Log}(y)=\text{Log}(x)+0.4 \text{ dex}$ relations are plotted as a black solid, dotted and dashed line, while the $N_{\text{H},z}=10^{24} \text{ cm}^{-2}$ threshold is plotted as a blue dashed line. The sources are color-coded by their number of degrees of freedom: blue sources have the fewest degrees of freedom, while red sources have the largest. A significant fraction of candidate CT-AGN with low-quality 0.5–10 keV data are reclassified as Compton thin when adding *NuSTAR* to the spectral analysis. *Right:* X-ray covering factor as a function of the difference between the logarithms of the line-of-sight and the average torus column density (ΔN_{H}) for 31 heavily obscured Seyfert 2 galaxies (Marchesi et al. 2019). Sources with 90% confidence lower boundary $f_{c,X}>0.55$ are plotted as red circles, sources with 90% confidence upper boundary $f_{c,X}<0.45$ are plotted as blue squares, and sources not belonging to either of the two classes are plotted as black stars. Sources with low $f_{c,X}$ have, on average, larger ΔN_{H} , which suggests that in these sources the obscuring material is patchy, rather than uniform.

the vast majority (up to 90 %) of AGNs are obscured, i.e., the accreting SMBHs are surrounded by a distribution of matter with column density $N_{\text{H},z}>10^{22} \text{ cm}^{-2}$. Obscuration in AGNs has been largely studied over the electromagnetic spectrum, from the optical (e.g., Lawrence 1991; Simpson 2005), to the infrared (see, e.g., Jaffe et al. 2004; Nenkova et al. 2008), and to the X-rays (e.g., Risaliti et al. 1999; Gilli et al. 2007; Marchesi et al. 2016c). Based on the results of these works, it is commonly accepted that the nuclear obscuration is caused by a so-called “dusty torus”, i.e., a distribution of molecular gas and dust located

at $\sim 1\text{--}10$ pc from the SMBH (e.g., Jaffe et al. 2004).

While the existence of obscuring material surrounding AGNs is universally accepted, its geometrical distribution and chemical composition, as well as its kinematics, are still matter of debate. Several works reported evidence pointing towards a “patchy torus” scenario, where the obscuring material is distributed in clumps formed by optically thick clouds (e.g., Jaffe et al. 2004; Elitzur & Shlosman 2006; Risaliti et al. 2007; Hönig & Beckert 2007; Nenkova et al. 2008; Risaliti et al. 2011; Burtscher et al. 2013; Zhao et al. 2020). Recently, high-sensitivity and high-spatial res-

olution ALMA observations confirmed that the obscuring medium is patchy, although on a limited number of objects (e.g., Imanishi et al. 2018). Multiwavelength observations also show that the obscuring medium is multi-phase and it can be either inflowing, thus feeding the accreting SMBH, or outflowing, during the so-called “feedback phase” (see, e.g., Tombesi et al. 2015; Tombesi 2016; Gaspari & Sadowski 2017; Gaspari et al. 2017). The study of the geometry, composition and kinematics of the obscuring material with a large sample of objects with excellent multiwavelength coverage, and the comparison between observations and hydrodynamical simulations of AGN feeding and feedback (e.g., Gaspari & Sadowski 2017), are key to understand and characterize the SMBH growth and how AGNs affect their host evolution across cosmic time.

With the aim of building a large sample of nearby, heavily obscured AGN to fully characterize the properties of the obscuring material, in Marchesi et al. (2017a,b) we presented a new, efficient method to find these elusive sources. We chose our objects among the AGN detected in the 15–150 keV band by *Swift*-BAT that were reported in the 100-month BAT catalog but still were lacking 0.5–10 keV data. To be selected as a candidate for our *Chandra* 0.5–7 keV follow-up campaign, a source should fulfil the following three criteria: *i*) Be a Seyfert 2 galaxy, since Seyfert 2 sources are on average more obscured than Seyfert 1s (see, e.g., Marchesi et al. 2016c); *ii*) Lack of a ROSAT counterpart in the 0.5–2.4 keV band, thus implying at least a moderate amount of obscuration (see Koss et al. 2015); *iii*) Have low redshift ($z \leq 0.04$, i.e., the redshift threshold below which $\sim 90\%$ of known candidate CT-AGN have been detected in previous works, see, e.g., Ricci et al. 2015). We then obtained a 5–10 ks *Chandra* follow-up of all the BAT sources meeting all these conditions.

We found these criteria to be highly effective, since all the selected objects have line-of-sight (l.o.s) column density $N_{\mathrm{H},z} > 10^{23} \mathrm{cm}^{-2}$: as a comparison, blindly selecting a source in the 36-month BAT catalog there is only a 30% chance to find such an obscured source (Burton et al. 2011). Furthermore, we found

two new candidate CT-AGN, which we then confirmed to be *bona fide* CT-AGN thanks to deep *NuSTAR* and *XMM-Newton* observations (Zhao et al. 2019a,b).

While the method described above is effective in finding new candidate heavily obscured AGN, short *Chandra* observations detect $\lesssim 100$ net counts in the 0.5–7 keV band, which are not enough to generate high-quality X-ray spectra. A proper characterization of these objects can be achieved only through the analysis of spectra with thousands of counts, and a proper coverage of the > 10 keV energy range, where most of the observed emission is. In other words, the proper characterization of low- z , heavily obscured AGN requires an extended follow-up campaign with *NuSTAR*.

Indeed, with the launch of the Nuclear Spectroscopic Telescope Array (*NuSTAR*, Harrison et al. 2013), the study and characterization of the physics of the obscuring material surrounding accreting SMBHs experienced a significant step forward. *NuSTAR* is the first telescope with focusing optics at > 10 keV, and its sensitivity is almost two orders of magnitude deeper than any of the other previous facilities in the same energy range. The observed X-ray emission of heavily obscured AGNs peaks at ~ 30 –50 keV (Ajello et al. 2008), where the so-called “Compton hump” is observed, while below 5 keV it is mostly absorbed (Koss et al. 2015). *NuSTAR*, covering the 3–78 keV energy range, is therefore the ideal instrument to investigate these otherwise elusive sources. The first years of *NuSTAR* were dedicated to the study of single, well-known Compton thick (CT, i.e., having line-of-sight, l.o.s, column density $N_{\mathrm{H},z} > 10^{24} \mathrm{cm}^{-2}$) AGNs, or to the characterization of small samples of heavily obscured sources (e.g., Baloković et al. 2014; Puccetti et al. 2014; Brightman et al. 2015; Masini et al. 2016). By 2018, however, the sample of heavily obscured AGNs observed by *NuSTAR* was finally large enough to study a statistically significant population of sources. We thus started a multi-year project with the goal of developing the most accurate characterization of the obscuring material in heavily obscured Seyfert 2 galaxies in the local Universe.

In Marchesi et al. (2018, 2019b), we analyzed the combined 2–70 keV spectra of 35 nearby ($d_L < 500$ Mpc; $\langle z \rangle = 0.03$) Seyfert 2 galaxies, all of which are candidate CT-AGN with archival *NuSTAR* data. 2–10 keV data have been obtained using archival XMM-*Newton*, *Chandra* and *Swift*-XRT data. We discovered a systematic trend to artificially overestimate the l.o.s. column density and the steepness of the spectrum when only the 2–10 keV and the *Swift*-BAT data are included in the fit (Fig. 3, left panel). This effect is variability– and model–independent and stronger in sources with low statistics (net cts < 100) in the 0.3–10 keV band, i.e., objects with only a *Swift*-XRT or a short (< 10 ks) *Chandra* spectrum available, where the l.o.s. column density is overestimated, on average, by $\sim 45\%$, while the average photon index variation is $\Delta\Gamma = 0.25$. As a consequence, only about half ($54^{+10}_{-13}\%$) of the candidate nearby CT-AGN reported in the literature are confirmed as bona-fide CT-AGN.

This result has important implications for our understanding of the CXB and the total accretion history of the Universe. For example, based on our results the observed CT-AGN fraction in the 70-month *Swift*-BAT catalog ($7.6^{+1.1}_{-2.1}\%$; Ricci et al. 2017), decreases to $6.0^{+0.4}_{-0.5}\%$ and potentially even down to $\sim 4\%$, extrapolating the results of our work to the population of candidate CT-AGN with no public *NuSTAR* data available. Notably, the low- z observed and intrinsic CT-AGN fractions play an important role in supermassive black hole population synthesis and CXB models (see, e.g., Ananna et al. 2019), and the total contribution of CT-AGN to the CXB is still debated.

Given its unprecedented effective area in the 5–70 keV band, *NuSTAR* can not only be used to measure basic AGN spectral parameters such as $N_{\text{H},z}$ and Γ , but also the geometry of the obscuring torus and its covering factor (f_c), as well as the average column density of the torus ($N_{\text{H,tor}}$). In Marchesi et al. (2019b) we further studied our sample of 35 nearby candidate CT-AGN with *NuSTAR* data, this time using the **borus02** model (Baloković et al. 2018) to compute f_c and $N_{\text{H,tor}}$.

We found a tentative evidence of different trends between f_c and the difference between the average torus column density and the line-of-sight column density: as shown in Figure 3, right panel, the offset is larger in low- f_c objects, where the average column density is always smaller than the line-of-sight column density, than in high- f_c objects. These results are consistent with a scenario where low- f_c AGNs are more likely to have a patchy torus, while high- f_c AGNs are more likely to be obscured by a more uniform distribution of gas. A recent work by Zhao et al. (2020), based on the analysis of BAT-selected AGN with *NuSTAR* data, supported the evidence that the majority of the obscured AGN in the local Universe indeed have a clumpy torus.

We also observed an inverse trend between the torus covering factor and the AGN 2–10 keV luminosity, i.e., sources with higher f_c values have on average lower luminosities, although the f_c dispersion in sources in the same range of luminosity is large. Our results nicely agree with both the obscured AGN fraction with respect to the total population measured by Burlon et al. (2011) and Vasudevan et al. (2013) in samples of BAT-selected AGNs in the nearby Universe, and with the low- z CT fraction measurements made by Lanzuisi et al. (2018) and Ricci et al. (2015), thus confirming that the f_c of a source is also an indicator of the probability to observe that source as obscured (the higher the covering factor, the higher the probability), therefore f_c and f_{obs} can in principle be directly compared. This trend needs nonetheless to be further validated using a larger sample of sources, all observed with *NuSTAR* to properly constrain $N_{\text{H},z}$, f_c and $L_{2-10\text{keV}}$.

3.1. Future developments

While X-rays provide us with a very efficient way to characterize obscured AGN, they are still biased against heavily obscured objects ($N_{\text{H},z} \geq 10^{25} \text{ cm}^{-2}$). Notably, there is also observational evidence that the material responsible for the X-ray obscuration may not spatially coincide with the one that causes the optical extinction, since in a non-negligible, albeit mi-

norary fraction of sources the optical classification does not match the X-ray one (e.g., we observe hundreds of unobscured Seyfert 2 galaxies and obscured Seyfert 1s in X-ray surveys Marchesi et al. 2016c). Furthermore, in some AGN there is lack of evidence for neutral absorption or emission from a dusty torus, and the obscuring material seems to be structured as a high-column density ($N_{\mathrm{H},z} \geq 10^{23} \text{ cm}^{-2}$), clumpy, photo-ionized disk wind (e.g., Nardini et al. 2015; Tombesi et al. 2015; Smith et al. 2019).

For these reasons, we plan to complement our X-ray analysis using high-quality infrared observations: the vast majority of the low- z , heavily obscured AGN have both WISE photometry and *Spitzer* IRS spectroscopic data. It will therefore be possible to measure the torus covering factor in a second, independent way using dusty torus models based on the mid-infrared (mIR; ~ 7.5 – $13.5 \mu\text{m}$) spectral energy distribution (SED) fitting (see, e.g., Nenkova et al. 2008; Hönig & Kishimoto 2010; García-González et al. 2017).

In Fig. 4 we show, on the left, the X-ray spectra of three Compton thick AGN having tori with different covering factors; in the right panel of the same Figure, we instead show an example of how different $f_{c,\text{IR}}$ values significantly change the shape of the AGN SED at the wavelengths covered by WISE. With our multi-band analysis we will assess if the X-ray and MIR covering factors are consistent or they significantly differ, in the latter case implying that the X-ray and IR obscuration may take place in two different regions. As a pilot project, in Marchesi et al. (2019b) we compared the X-ray measurements we obtained for two objects, NGC 1068 and NGC 7582, with those derived in the MIR by Alonso-Herrero et al. (2011): we find that for both sources there is a remarkable agreement, within 10 %, between $f_{c,X}$ and $f_{c,\text{IR}}$.

We will also build on the results of a recent work by Esparza-Arredondo et al. (2019), which for the first time jointly fitted the X-ray and *Spitzer* IR spectra of the heavily obscured Type 2 AGN IC 5063, and measure the properties of the obscuring torus in a self-consistent way using both the X-ray model

borus02 (Baloković et al. 2018) and the Fritz et al. (2006) midIR torus model.

To complement our analysis of SMBH obscured accretion, we will study if and how the nuclear obscuration is linked to the amount of gas available in the host, M_{gas} , and analyze how AGN feedback affects the host galaxy. More specifically, we will determine how the depletion time of the host, i.e., the ratio between the mass of cold gas and the star formation rate ($t_{\mathrm{depl}} = M_{\mathrm{gas}}/\mathrm{SFR}$) varies when an AGN is present in the galaxy. If the AGN can completely remove or heat the gas, thus preventing it from cooling, we would expect low host depletion time ($t_{\mathrm{depl}} = M_{\mathrm{gas}}/\mathrm{SFR}$, where M_{gas} is the host gas mass and SFR is its star formation rate) values with respect to inactive galaxies with similar stellar masses (M_{\star}) and SFR. Indeed, low t_{depl} ($0.01 < t_{\mathrm{depl}} < 0.1$ Gyrs), i.e., lower than in normal galaxies with similar SFR and M_{\star} , have already been found in luminous AGN at high z (i.e. $z \sim 1.5$ – 2.5 ; see, e.g., Brusa et al. 2018; Perna et al. 2018), while in the local Universe our knowledge on the topic is still limited (see, e.g., Casasola et al. 2015; Rosario et al. 2018). A first example of this type of analysis is reported in Pozzi et al. (2017), where *NuSTAR*, *Chandra* and ALMA data was combined to characterize the CT Seyfert 2 galaxy NGC 7130, a source which is also part of the Marchesi et al. (2018) sample.

4. A look to the future: new facilities for new science

As already discussed in the previous sections, 20 years of observations with *Chandra* and XMM-Newton built large samples of X-ray selected AGNs. This allowed us to put constraints on the co-evolution of the accreting supermassive black holes and their host galaxies, starting from the local Universe and sampling with good statistic the overall AGN population up to the peak of both AGN and star-formation activity ($z \sim 2$). Unfortunately, moving towards higher redshifts current X-ray facilities become much less effective. In particular, our knowledge on the origin and growth of the first population of AGN, those which were

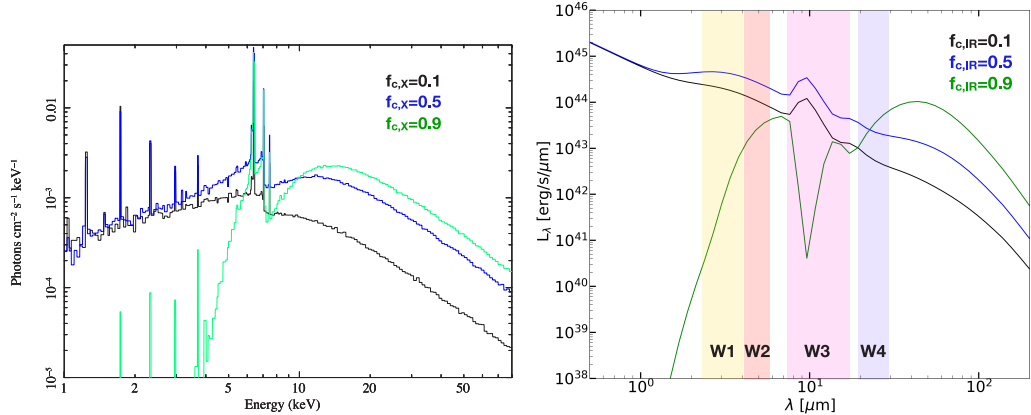


Fig. 4. *Left:* X-ray spectral energy distribution (SED) of a heavily obscured AGN ($N_{\text{H,tor}}=10^{24}$ cm⁻²) at $z=0$, for three different tori covering factors. A proper measurement of $f_{c,X}$ requires high quality data in the 0.5–10 keV (i.e., *XMM-Newton* data) and at energies >10 keV (i.e., *NuSTAR* data). *Right:* Infrared SED of a torus for the same covering factors shown in the left panel: the four WISE bandwidths are also overplotted. WISE data, used in synergy with available optical and *Spitzer* information, will allow us to properly measure $f_{c,IR}$.

formed in the 2 Gyr after the Big Bang (i.e., at redshift $z > 3$) is still limited (see, e.g., Ueda et al. 2014; Aird et al. 2015; Buchner et al. 2015; Miyaji et al. 2015; Ananna et al. 2019). The overall sample of X-ray selected AGNs detected at $z > 3$ contains only ~ 300 sources (see, e.g., Vito et al. 2014, 2018; Marchesi et al. 2016b), and the farthest spectroscopically confirmed X-ray selected AGN has been found at $z=5.31$ (Capak et al. 2011). It is also worth noting that the vast majority of these high- z X-ray sources are simply detected, meaning that their count statistic does not allow us to perform a proper spectral fit, thus further limiting the scientific outcome of their analysis. In particular, studying the evolution with redshift of the fraction of obscured AGNs (which has been shown to increase with redshift in several works, see, e.g., Treister et al. 2013; Vito et al. 2018) becomes particularly complex, since it requires the introduction of significant incompleteness corrections (see, e.g., Lanzuisi et al. 2018). Notably, while obscured AGN are expected to make the majority of the high- z AGN population, at $z > 6$ optical/NIR surveys have so far detected only unobscured, luminous quasars (Bañados et al. 2016; Wang et al.

2017). As extensively discussed in the previous sections, a proper X-ray spectral characterization of heavily obscured AGNs requires the detection of hundreds of source counts (see, e.g., Marchesi et al. 2018, 2019b), a task that cannot be achieved by current X-ray telescopes.

For these reasons, a new generation of X-ray facilities is required to shed light on the formation and evolution of the first accreting supermassive black holes, and complement the information that will become available in the next decade in the other bands. To properly assess the ideal technical layout for these future facilities, one needs to perform extensive X-ray survey simulations. This is what we did in Marchesi et al. (2020). We first built mock catalogs of active galactic nuclei, derived from the AGN population synthesis models by Gilli et al. (2007) and Vito et al. (2014, for the high-redshift, $z > 3$ population); non-active galaxies, derived from the Ranalli et al. (2005) number counts; and clusters of galaxies, based on the predictions of dark matter halos extracted from the numerical mass function by Tinker et al. (2008) and Despali et al. (2016).

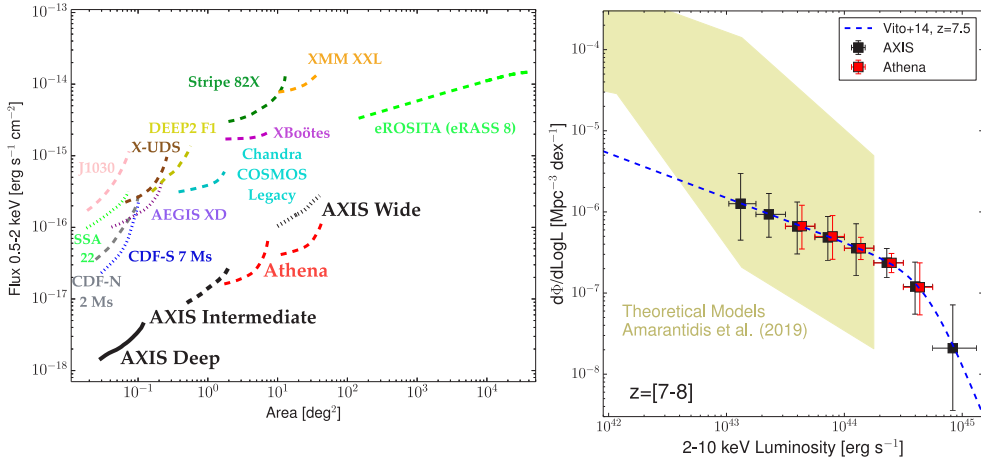


Fig. 5. *Left:* Predicted 0.5–2 keV area-flux curves for the AXIS deep, 5 Ms (black solid line), intermediate, 300 ks (black dashed line) and wide, 15 ks (black dotted line) proposed surveys, and for the *Athena* deep– and wide-area survey. For comparison, we show the area-flux curves of several existing X-ray surveys. As can be seen, AXIS and *Athena* will work in synergy to explore a totally new region of the area-flux plane, thus allowing us to enormously improve our AGN knowledge, especially with regard to the high- z and the heavily obscured population. *Right:* AXIS (black) and *Athena* (red) simulated X-ray luminosity functions at $z \sim 7.5$. The X-ray luminosity function at the same redshift derived by Vito et al. (2014) extrapolating the results obtained at $z=[3-5.5]$ using *Chandra*-detected AGN is plotted as a blue dashed line. We also show, for comparison, the range of predictions from the hydro-dynamical simulations and semi-analytical models discussed in Amarantidis et al. (2019, khaki area). As can be seen, AXIS and *Athena* will offer an unprecedented accuracy in this range of redshifts and luminosities, thus enabling an accurate tuning of the theoretical models. Plots from Marchesi et al. (2020).

We then used these mock catalogs¹ to simulate X-ray surveys with the *Athena* Wide Field Imager (WFI; Nandra et al. 2013; Meidinger et al. 2017) and with the AXIS probe (Mushotzky et al. 2019). The *Athena* WFI will have 40'-diameter DEPFET chips, and will be the instrument with the largest effective area in the 0.3–10 keV band. WFI will also benefit from an impressively stable, $\sim 5\text{--}6''$ half-energy width over the whole field of view. AXIS is a probe-class mission proposed to the Decadal Survey on Astronomy and Astrophysics 2020, with 0.3–10 keV observing band pass and sub-arcsecond resolu-

tion over an area of over 500 square arcminutes, which is, over a $24'\times 24'$ field of view.

As shown in Figure 5, left panel, AXIS and *Athena* would reach unprecedented fluxes, thus opening a new window of knowledge in AGN formation and evolution. Overall, the two instruments would detect up to $\sim 500,000$ X-ray sources: about 85 % of these objects are expected to be AGNs, while the remaining 15 % (i.e., $\sim 70,000$ sources), are expected to be non-active galaxies. Based on a comparison with currently available X-ray surveys, ~ 90 % of these objects would be detected in the X-rays for the first time.

Even more importantly, we expect to detect over 20,000 AGNs at $z > 3$, which is, a factor ~ 60 more than those detected with cur-

¹ Available online at <http://cxb.oas.inaf.it/mock.html>.

rent X-ray facilities. For the first time, it would also be possible to detect a significant (several hundred of sources) population of X-ray detected AGN at $z > 6$. In Figure 5, right panel, we show the simulated AXIS and *Athena* X-ray luminosity functions at $z \sim 7.5$, together with the range of predictions of several different models of SMBH early accretion, both hydrodynamical (namely, EAGLE, Crain et al. 2015; Schaye et al. 2015; McAlpine et al. 2016, Horizon-AGN, Dubois et al. 2014, Illustris, Vogelsberger et al. 2014, and MassiveBlackII, Khandai et al. 2015) and semi-analytical (GALFORM, Cole et al. 2000; Lacey et al. 2016, L-Galaxies Guo et al. 2011; Henriques et al. 2015, MERAXES Mutch et al. 2016; Qin et al. 2017, and SHARK Lagos et al. 2018). The range of predictions has been taken from Amarantidis et al. (2019), to which we refer for a complete description of the models. As it can be seen, the almost complete lack of observationally confirmed accreting supermassive black holes at $z > 7$ is reflected in the predictions of the theoretical models of black hole creation and early growth. AXIS and *Athena* would significantly help in addressing this issue, even without directly detecting the first black hole seeds at $z \gtrsim 20$: indeed, constraining the AGN $z \sim 7$ XLF with uncertainties $< 50\%$ over a wide range of luminosities will still allow for an unprecedented tuning of the theoretical SMBH accretion models.

The detection of an unprecedented number of X-ray detected AGNs will require a similarly unprecedented effort in terms of counterpart identification and redshift measurement. This challenge will be particularly though for the subsample of sources which are the most intriguing, which is., high-redshift and/or heavily obscured AGNs. As a consequence, next-generation X-ray surveys will then need to be complemented with an extended optical/infrared follow-up effort. For example, Comparat et al. (2019) discussed the most efficient way to build large spectroscopic campaigns with all kind of facilities, from 1m to 8m+ telescopes mounting efficient multi-object spectrographs (such as, e.g., 4MOST, de Jong et al. 2012, DESI, DESI Collaboration et al. 2016; VIMOS, Scudeggio et al. 2005;

MUSE, Bacon et al. 2015). To ensure that the vast majority of the X-ray detected sources will have a counterpart and a photometric redshift, large-area photometric surveys with facilities such as LSST and the Roman Space Telescope will also play a key role (see, e.g., Hemmati et al. 2019).

References

- Aird, J., Coil, A. L., Georgakis, A., et al. 2015, MNRAS, 451, 1892
- Ajello, M., Greiner, J., Sato, G., et al. 2008, ApJ, 689, 666
- Alexander, D. M. & Hickox, R. C. 2012, NAr, 56, 93
- Allevato, V., Civano, F., Finoguenov, A., et al. 2016, ApJ, 832, 70
- Allevato, V., Finoguenov, A., Civano, F., et al. 2014, ApJ, 796, 4
- Allevato, V., Viitanen, A., Finoguenov, A., et al. 2019, A&A, 632, A88
- Alonso-Herrero, A., Ramos Almeida, C., Mason, R., et al. 2011, ApJ, 736, 82
- Amarantidis, S., Afonso, J., Messias, H., et al. 2019, MNRAS, 485, 2694
- Ananna, T. T., Treister, E., Urry, C. M., et al. 2019, ApJ, 871, 240
- Bañados, E., Venemans, B. P., Decarli, R., et al. 2016, ApJS, 227, 11
- Bacon, R., Brinchmann, J., Richard, J., et al. 2015, A&A, 575, A75
- Ballantyne, D. R., Everett, J. E., & Murray, N. 2006, ApJ, 639, 740
- Baloković, M., Brightman, M., Harrison, F. A., et al. 2018, ApJ, 854, 42
- Baloković, M., Comastri, A., Harrison, F. A., et al. 2014, ApJ, 794, 111
- Brightman, M., Baloković, M., Stern, D., et al. 2015, ApJ, 805, 41
- Brusa, M., Cresci, G., Daddi, E., et al. 2018, A&A, 612, A29
- Buchner, J., Georgakis, A., Nandra, K., et al. 2015, ApJ, 802, 89
- Burlon, D., Ajello, M., Greiner, J., et al. 2011, ApJ, 728, 58
- Burtscher, L., Meisenheimer, K., Tristram, K. R. W., et al. 2013, A&A, 558, A149
- Capak, P. L., Riechers, D., Scoville, N. Z., et al. 2011, Nature, 470, 233

- Casasola, V., Hunt, L., Combes, F., & García-Burillo, S. 2015, A&A, 577, A135
- Circosta, C., Vignali, C., Gilli, R., et al. 2019, A&A, 623, A172
- Cisternas, M., Gadotti, D. A., Knapen, J. H., et al. 2013, ApJ, 776, 50
- Civano, F., Hickox, R. C., Puccetti, S., et al. 2015, ApJ, 808, 185
- Cole, S., Lacey, C. G., Baugh, C. M., & Frenk, C. S. 2000, MNRAS, 319, 168
- Comastri, A., Ranalli, P., Iwasawa, K., et al. 2011, A&A, 526, L9
- Comparat, J., Merloni, A., Salvato, M., et al. 2019, MNRAS, 487, 2005
- Crain, R. A., Schaye, J., Bower, R. G., et al. 2015, MNRAS, 450, 1937
- de Jong, R. S., Bellido-Tirado, O., Chiappini, C., et al. 2012, in Society of Photo-Optical Instrumentation Engineers (SPIE) Conference Series, Vol. 8446, Proc. SPIE, 84460T
- Del Moro, A., Mullaney, J. R., Alexander, D. M., et al. 2014, ApJ, 786, 16
- DESI Collaboration, Aghamousa, A., Aguilar, J., et al. 2016, arXiv e-prints, arXiv:1611.00036
- Despali, G., Giocoli, C., Angulo, R. E., et al. 2016, MNRAS, 456, 2486
- Donley, J. L., Koekemoer, A. M., Brusa, M., et al. 2012, ApJ, 748, 142
- Donley, J. L., Rieke, G. H., Pérez-González, P. G., & Barro, G. 2008, ApJ, 687, 111
- Dubois, Y., Pichon, C., Welker, C., et al. 2014, MNRAS, 444, 1453
- Elitzur, M. & Shlosman, I. 2006, ApJ, 648, L101
- Esparza-Arredondo, D., González-Martín, O., Dultzin, D., et al. 2019, ApJ, 886, 125
- Fritz, J., Franceschini, A., & Hatziminaoglou, E. 2006, MNRAS, 366, 767
- García-González, J., Alonso-Herrero, A., Höning, S. F., et al. 2017, MNRAS, 470, 2578
- Gaspari, M. & Sadowski, A. 2017, ApJ, 837, 149
- Gaspari, M., Temi, P., & Brighenti, F. 2017, MNRAS, 466, 677
- Georgantopoulos, I., Comastri, A., Vignali, C., et al. 2013, A&A, 555, A43
- Giallongo, E., Grazian, A., Fiore, F., et al. 2015, A&A, 578, A83
- Gilli, R., Comastri, A., & Hasinger, G. 2007, A&A, 463, 79
- Guo, Q., White, S., Boylan-Kolchin, M., et al. 2011, MNRAS, 413, 101
- Harrison, F. A., Craig, W. W., Christensen, F. E., et al. 2013, ApJ, 770, 103
- Hasinger, G. 2008, A&A, 490, 905
- Hemmati, S., Capak, P., Masters, D., et al. 2019, ApJ, 877, 117
- Henriques, B. M. B., White, S. D. M., Thomas, P. A., et al. 2015, MNRAS, 451, 2663
- Hönig, S. F. & Beckert, T. 2007, MNRAS, 380, 1172
- Hönig, S. F. & Kishimoto, M. 2010, A&A, 523, A27
- Imanishi, M., Nakanishi, K., Izumi, T., & Wada, K. 2018, ApJ, 853, L25
- Jaffe, W., Meisenheimer, K., Röttgering, H. J. A., et al. 2004, Nature, 429, 47
- Khandai, N., Di Matteo, T., Croft, R., et al. 2015, MNRAS, 450, 1349
- Koss, M. J., Romero-Cañizales, C., Baronchelli, L., et al. 2015, ApJ, 807, 149
- La Franca, F., Fiore, F., Comastri, A., et al. 2005, ApJ, 635, 864
- Lacey, C. G., Baugh, C. M., Frenk, C. S., et al. 2016, MNRAS, 462, 3854
- Lagos, C. d. P., Tobar, R. J., Robotham, A. S. G., et al. 2018, MNRAS, 481, 3573
- Lansbury, G. B., Alexander, D. M., Del Moro, A., et al. 2014, ApJ, 785, 17
- Lanzuisi, G., Civano, F., Marchesi, S., et al. 2018, MNRAS, 480, 2578
- Lanzuisi, G., Delvecchio, I., Berta, S., et al. 2017, A&A, 602, A123
- Lanzuisi, G., Ranalli, P., Georgantopoulos, I., et al. 2015, A&A, 573, A137
- Lawrence, A. 1991, MNRAS, 252, 586
- Lehmer, B. D., Xue, Y. Q., Brandt, W. N., et al. 2012, ApJ, 752, 46
- Madau, P. & Haardt, F. 2015, ApJ, 813, L8
- Marchesi, S., Ajello, M., Comastri, A., et al. 2017a, ApJ, 836, 116
- Marchesi, S., Ajello, M., Marcotulli, L., et al. 2018, ApJ, 854, 49
- Marchesi, S., Ajello, M., Zhao, X., et al. 2019a, ApJ, 882, 162
- Marchesi, S., Ajello, M., Zhao, X., et al.

- 2019b, *ApJ*, 872, 8
 Marchesi, S., Civano, F., Elvis, M., et al.
 2016a, *ApJ*, 817, 34
 Marchesi, S., Civano, F., Salvato, M., et al.
 2016b, *ApJ*, 827, 150
 Marchesi, S., Gilli, R., Lanzuisi, G., et al.
 2020, *A&A*, 642, A184
 Marchesi, S., Lanzuisi, G., Civano, F., et al.
 2016c, *ApJ*, 830, 100
 Marchesi, S., Tremblay, L., Ajello, M., et al.
 2017b, *ApJ*, 848, 53
 Masini, A., Comastri, A., Baloković, M., et al.
 2016, *A&A*, 589, A59
 Masters, D., Capak, P., Salvato, M., et al. 2012,
 ApJ, 755, 169
 McAlpine, S., Helly, J. C., Schaller, M., et al.
 2016, *Astronomy and Computing*, 15, 72
 McGreer, I. D., Jiang, L., Fan, X., et al. 2013,
 ApJ, 768, 105
 Meidinger, N., Barbera, M., Emberger, V., et al. 2017, in *Society of Photo-Optical Instrumentation Engineers (SPIE) Conference Series*, Vol. 10397, Proc. SPIE, 103970V
 Miyaji, T., Hasinger, G., Salvato, M., et al.
 2015, *ApJ*, 804, 104
 Mushotzky, R. F., Aird, J., Barger, A. J., et al.
 2019, arXiv e-prints, arXiv:1903.04083
 Mutch, S. J., Geil, P. M., Poole, G. B., et al.
 2016, *MNRAS*, 462, 250
 Nandra, K., Barret, D., Barcons, X., et al. 2013,
 arXiv e-prints, arXiv:1306.2307
 Nardini, E., Reeves, J. N., Gofford, J., et al.
 2015, *Science*, 347, 860
 Nenkova, M., Sirocky, M. M., Ivezić, Ž., &
 Elitzur, M. 2008, *ApJ*, 685, 147
 Perna, M., Sargent, M. T., Brusa, M., et al.
 2018, *A&A*, 619, A90
 Pozzi, F., Vallini, L., Vignali, C., et al. 2017,
 MNRAS, 470, L64
 Puccetti, S., Comastri, A., Fiore, F., et al. 2014,
 ApJ, 793, 26
 Qin, Y., Mutch, S. J., Poole, G. B., et al. 2017,
 MNRAS, 472, 2009
 Ranalli, P., Comastri, A., & Setti, G. 2005,
 A&A, 440, 23
 Ricci, C., Ueda, Y., Koss, M. J., et al. 2015,
 ApJ, 815, L13
 Ricci, F., Marchesi, S., Shankar, F., La Franca,
 F., & Civano, F. 2017, *MNRAS*, 465, 1915
 Risaliti, G., Elvis, M., Fabbiano, G., et al.
 2007, *ApJ*, 659, L111
 Risaliti, G., Maiolino, R., & Salvati, M. 1999,
 ApJ, 522, 157
 Risaliti, G., Nardini, E., Salvati, M., et al. 2011,
 MNRAS, 410, 1027
 Rodighiero, G., Brusa, M., Daddi, E., et al.
 2015, *ApJ*, 800, L10
 Rosario, D. J., Burtscher, L., Davies, R. I., et al.
 2018, *MNRAS*, 473, 5658
 Rosario, D. J., Santini, P., Lutz, D., et al. 2012,
 A&A, 545, A45
 Ross, N. P., McGreer, I. D., White, M., et al.
 2013, *ApJ*, 773, 14
 Rovilos, E., Comastri, A., Gilli, R., et al. 2012,
 A&A, 546, A58
 Schaye, J., Crain, R. A., Bower, R. G., et al.
 2015, *MNRAS*, 446, 521
 Scoville, M., Franzetti, P., Garilli, B., et al.
 2005, *PASP*, 117, 1284
 Shao, L., Lutz, D., Nordon, R., et al. 2010,
 A&A, 518, L26
 Shen, Y. 2009, *ApJ*, 704, 89
 Simpson, C. 2005, *MNRAS*, 360, 565
 Smith, R. N., Tombesi, F., Veilleux, S.,
 Lohfink, A. M., & Luminari, A. 2019, *ApJ*,
 887, 69
 Stern, D., Assef, R. J., Benford, D. J., et al.
 2012, *ApJ*, 753, 30
 Tinker, J., Kravtsov, A. V., Klypin, A., et al.
 2008, *ApJ*, 688, 709
 Tombesi, F. 2016, *Astronomische Nachrichten*,
 337, 410
 Tombesi, F., Meléndez, M., Veilleux, S., et al.
 2015, *Nature*, 519, 436
 Treister, E., Schawinski, K., Volonteri, M., &
 Natarajan, P. 2013, *ApJ*, 778, 130
 Ueda, Y., Akiyama, M., Hasinger, G., Miyaji,
 T., & Watson, M. G. 2014, *ApJ*, 786, 104
 Vito, F., Brandt, W. N., Yang, G., et al. 2018,
 MNRAS, 473, 2378
 Vito, F., Gilli, R., Vignali, C., et al. 2014,
 MNRAS, 445, 3557
 Vogelsberger, M., Genel, S., Springel, V., et al.
 2014, *MNRAS*, 444, 1518
 Wang, F., Fan, X., Yang, J., et al. 2017, *ApJ*,
 839, 27
 Zhao, X., Marchesi, S., & Ajello, M. 2019a,
 ApJ, 871, 182
 Zhao, X., Marchesi, S., Ajello, M., et al. 2020,

arXiv e-prints, arXiv:2011.03851
Zhao, X., Marchesi, S., Ajello, M., et al.
2019b, ApJ, 870, 60